Experimental Thermal and Fluid Science 92 (2018) 270–285

Contents lists available at ScienceDirect

Experimental Thermal and Fluid Science

journal homepage: www.elsevier.com/locate/etfs

Experimental study of viscosity effects on heavy crude oil-water core-annular flow pattern

Caio A.M. Cavicchio[a,*], Jorge L. Biazussi[a], Marcelo S. de Castro[b], Antonio C. Bannwart[b], Oscar M.H. Rodriguez[c], Carlos H.M. de Carvalho[d]

[a] Center for Petroleum Studies, University of Campinas – UNICAMP, Campinas, SP, Brazil
[b] Department of Energy, Faculty of Mechanical Engineering, University of Campinas – UNICAMP, Campinas, SP, Brazil
[c] Department of Mechanical Engineering, São Carlos School of Engineering, University of São Paulo – USP, São Carlos, SP, Brazil
[d] CENPES/PETROBRAS, Rio de Janeiro, RJ, Brazil

ARTICLE INFO

Keywords:
Two-phase flow
Heavy crude oil
Core-annular flow
Pressure drop

ABSTRACT

It is well known that in multiphase flow, different flow patterns lead to different pressure gradients. One remarkable example is the oil-water core-annular flow with water in the annulus and viscous oil in the core. Researchers have thus studied this flow pattern as a possible artificial lift technique for the production and transport of crudes and/or petroleum mixtures of high viscosities, which application might imply in energy efficiency increase and costs reduction for the oil industry. Hence, in this work, a set of experiments with vertical-upward heavy crude oil–water flows were carried out to study the influence of viscosity on the core-annular flow parameters. The oil was diluted with diesel to present tests with oil viscosities of 557, 1112, 1561, and 1729 cP and tap water as working fluids in a vertical 59-mm-i.d. and 13-m-length test section. The slip ratio between phases and holdup were obtained by a slow-motion footage technique and compared with literature models. The measured core-annular flow frictional pressure gradient had the same magnitude of water single-phase flow at the mixture flow rate and total pressure gradient was smaller than for single-phase oil flow. Total reduction factors up to four times were observed. Minimum oil holdup for core-annular flow exists, having an oil viscosity influence and its effects on flow parameters were presented.

1. Introduction

The recent discoveries of oil reserves offshore of Brazil have important worldwide implications. Lying beneath great depths of water, these reserves call for more technical and technological efforts to make them economically viable. This has made attractive certain unconventional oil resources that have been known about but are still untapped because of low profitability motifs, such as oil sands and extra-heavy crude oil around the world – estimated to contain 1 to 1.5 trillion barrels [1].

Amongst the methods to produce and transport heavy oil, the two most common are to heat the fluid periodically along the pipeline and to add lighter oil to the fluid, acting as a dilutent agent. The first method demands a lot of energy; the second calls for lighter oil to be available in the surroundings. A key to resolving the problems associated with such issues may be decreasing the high pressure gradient associated with the friction between the fluid and the pipeline. This type of friction is one of the main factors that make it necessary to use high pumping energy.

If, as an annulus, a thin film of water is injected along the wall of the pipeline, this film manages to keep the oil core away from the pipe wall. The pressure drop is much lower than that of single-phase flow and, in some cases, can even be of the same order as water single-phase flow. This flow pattern, referred to as core-annular flow, has been subject of research since the 1940s, with early patents going to Isaac and Speed [2], Clark and Shapiro [3] and the works of Russel and Charles [4], Charles et al. [5], Ooms [6], Oliemans [7], Ho and Li [8], Bannwart [9], Prada [10], Rodriguez [11] and Biazussi [12].

Prada [10] studied horizontal and upward-vertical core-annular flows and collected pressure-gradient data with an oil 15,000 times as viscous as water. The author observed that the frictional pressure drop was reduced by 1287 times, while the total pressure drop by 93 times. These represent important data concerning the production and transport of petroleum. Other authors such as Rodriguez [11], Joseph et al. [13], Bai [14] and Bannwart [9] did the same, analysing the pressure drop associated with the core-annular flow pattern and presenting ways

* Corresponding author.
E-mail addresses: caio_cavicchio@hotmail.com (C.A.M. Cavicchio), jorge.biazussi@gmail.com (J.L. Biazussi), mcastro@fem.unicamp.br (M.S. de Castro), bannwart@dep.fem.unicamp.br (A.C. Bannwart), oscarmhr@sc.usp.br (O.M.H. Rodriguez), chmc@petrobras.com.br (C.H.M. de Carvalho).

https://doi.org/10.1016/j.expthermflusci.2017.11.027
Received 3 July 2017; Received in revised form 28 November 2017; Accepted 30 November 2017
Available online 02 December 2017
0894-1777/

Nomenclature

A	cross sectional area [m^2]
A_W	water cross sectional area occupied [m^2]
A_O	oil cross sectional area occupied [m^2]
a	constant for density correction due temperature [g/cm^3.°C]
f_W	water fraction in oil [–]
g	acceleration of gravity [m^2/s]
h	height between points 1 and 2 [m]
J_M	mixture velocity [m/s]
J_W	water superficial velocity [m/s]
J_O	oil superficial velocity [m/s]
P_1	pressure at point 1 [Pa]
P_2	pressure at point 2 [Pa]
P_1'	pressure at Validyne™ related to point 1
P_2'	pressure at Validyne™ related to point 2
Q_W	water flow rate [m^3/s]
Q_O	oil flow rate [m^3/s]
s	slip ratio [–]
s_{exp}	experimental slip [–]
s_{calc}	calculated slip [–]
T	temperature [°C]
u_x	propagated standard uncertainty on height x
u_y	estimated standard uncertainty of y
u_z	estimated standard uncertainty of z
V_W	water phase velocity [m/s]
V_O	oil phase velocity [m/s]

Greek

Γ_f	frictional pressure gradient [Pa/m]
$\Gamma_{f\ water}$	water frictional pressure gradient [Pa/m]
$\Gamma_{f\ oil}$	oil frictional pressure gradient [Pa/m]
$\Gamma_{f\ core\ flow}$	frictional pressure gradient in CAF [Pa/m]
$\Gamma_{t\ core\ flow}$	total pressure gradient in CAF [Pa/m]
$\frac{\Gamma_{f\ oil}}{\Gamma_{f\ core\ flow}}$	reduction factor [–]
$\frac{\Gamma_{t\ oil}}{\Gamma_{t\ core\ flow}}$	total reduction factor [–]
ΔP_f	frictional pressure loss [Pa]
ε_W	water holdup [–]
ε_O	oil holdup [–]
$\varepsilon_{O,exp}$	experimental oil holdup [–]
$\varepsilon_{O,calc}$	calculated oil holdup [–]
ρ_W	water density [g/cm^3]
ρ_O	oil density [g/cm^3]
ρ_m	mixture density [g/cm^3]
ρ_e	emulsion density [g/cm^3]
$\rho_O(0°)$	oil density at 0 °C [g/cm^3]

Abbreviations

CAF	core-annular flow

to determine important flow characteristics such as the slip ratio and holdup.

The main objective of the present work is to study the frictional and total pressure gradients of upward vertical core-annular flow, with four different viscosities of a heavy crude oil diluted with diesel. Data regarding oil holdup, in-situ oil velocity, interfacial wave speed, and slip ratio were acquired and compared with Rodriguez's [11] models. A high-speed video camera was used along with a technique from Biazussi [12] to treat the images. The frictional pressure gradient was measured with differential pressure transducers from *Validyne*™.

Considering a simultaneous two-phase flow of water and oil in a pipeline with a cross sectional area A and flow rates of water and oil given by Q_W and Q_O, the mixture velocity, J_M, can be defined as follows:

$$J_M = \frac{Q_W + Q_O}{A} = J_W + J_O \tag{1.1}$$

where J_W and J_O are the superficial velocities of water and oil, respectively, defined by Eq. (1.2):

$$J_W = \frac{Q_W}{A}; \quad J_O = \frac{Q_O}{A} \tag{1.2}$$

Labelling A_W and A_O as the real areas of the pipe occupied by water and oil, respectively, the real velocities are defined as:

$$V_W = \frac{Q_W}{A_W}; \quad V_O = \frac{Q_O}{A_O} \tag{1.3}$$

The in-situ volumetric fractions of the fluids (i.e., the volumetric fraction in the pipeline) are defined as holdups—ε_W for water and ε_O for oil.

$$\varepsilon_W = \frac{A_W}{A}; \quad \varepsilon_O = \frac{A_O}{A} \tag{1.4}$$

Differences in densities and/or viscosities of the fluids in the pipeline lead to the appearance of an important feature of multiphase flows, the slip ratio, s, of one phase relative to the other. Oliemans [7] described the slip ratio as the ratio between the water-oil in-situ volumetric ratio (holdup ratio) and the flow-rate ratio, in his work presented as Eq. (1.5):

$$s = \frac{V_O}{V_W} = \frac{\varepsilon_W/\varepsilon_O}{Q_W/Q_O} = \frac{J_O}{J_W} * \left(\frac{1-\varepsilon_O}{\varepsilon_O}\right) \tag{1.5}$$

Slip ratio values below unity means the oil phase is "accumulating" in the pipe; values above unity means water is "accumulating" in the pipeline.

Premanadhan [15] studied experimentally the oil-water two-phase flow of two oils of different viscosities, a light oil of 30 cP and a heavy oil of 300 cP in a 27.86-mm pipeline. The main objectives studied were flow patterns and pressure drop. Premanadhan reported that it was not possible to observe the core-annular flow, due to the high superficial-velocity ratio needed. On the other hand, seven different liquid-liquid flow patterns were observed, with changes at the transition boundaries due to the oil viscosity.

Zhang, Sarica and Pereyra [16] performed an oil multiphase pipe flow review, by comparing high-viscosity with low-viscosity oil experimental data – from two phase oil/gas and oil/water flows, to three phase oil/water/gas flow. The authors found significant discrepancies between them regarding interfacial waves structures and phase distributions, for example. Moreover, it was verified that the available mechanistic multiphase flow models do not predict well for high-viscosity oil. Focus on individual closure relationships were suggested.

Shi et al. [17] performed experimental tests and modelling of horizontal water-lubricated transport of high-viscosity oils flows. Experimental data taken were compared with some modelling predictions present at the literature, for water holdup and pressure gradient. Differences among them were discussed, with some modifications in an empirical correlation for water holdup made to show more accurate predictions. Oil fouling difficult accounting was indicated as the reason for the pressure gradient predictions deviations.

2. Experimental setup and procedure

The experiments with the heavy crude oil were carried out in the experimental setup of the Experimental Laboratory of Petroleum, LabPetro of the Center for Petroleum Studies – CEPETRO – at the

University of Campinas in Brazil. The heavy crude oil used in the experiments was originally from one of Brazil's onshore oilfields; it had a viscosity of around 34 Poise and a density of 970.3 kg/m^3 at 25 °C. The water used for the experiments was tap water, density depending on temperature following the work of Wagner & Pruß [18] and viscosity of 1 cP.

2.1. Experimental setup

The overall height of the experimental setup from the injection nozzle to the gravitational separator tank was 13 m. The gravitational separator tank located on the laboratory's rooftop gave rise to two liquid pipelines—one for water and one for oil. The water pipeline had a centrifugal pump and a Coriolis mass flow meter, an Emerson Micro Motion F series F200, with a maximum measurement capacity of 725 kg/min and 0.2% of uncertainty of the measure. After being pumped and its mass flowrate measured, water flowed to the injection nozzle and then to the test section of 59 mm i.d. The oil pipeline was equipped with a progressive cavity pump, and a Roxar WaterCut Meter FullCut with 1.5% of uncertainty of the measure that was used to measure the watercut. The same equipment counted with a PT100 sensor for temperature and had a measure uncertainty of 0.75%. The oil mass flowrate was measured with a Coriolis meter from Metroval model RHM40 with maximum measurement capacity of 900 kg/min and a measure uncertainty of 0.15%. After the water and oil were pumped and the mass flowrates, temperature, and watercut measured, the fluids entered the test section through the injection nozzle to produce the two-phase flow. The two-phase test section was equipped with a Rosemount model 2088 manometric pressure transducer with a measuring capacity of up to 20 bar and 0.1% measurement uncertainty and a *Validyne*™ differential pressure transducer, model DP15 with diaphragm #24, maximum capacity of measurement of 2.2 kPa and 0.25% measurement uncertainty. Movies of the flow were recorded at the visualization section, which to reduce lens effects was made of a glass pipe with an acrylic box filled with water. The fluids then flowed back to the gravity separator tank. Fig. 1 offers an illustrative sketch of the setup.

The experimental setup was validated with water single-phase flow and compared with friction factors found in the literature. This step was essential for checking the calibrations of all instruments and for further use of the setup for the core-annular flow-pattern experiments.

2.2. Commissioning of the experimental system

Prior to check up for correct apparatus operation, the separation tank was filled with water and the pumps functioning were checked at low rotations, separately. To ensure proper functioning, a pressure loss curve at different water volumetric flows was obtained. The aim was to compare the measured data with known correlations for friction factor from the literature, such as the Colebrook's correlation (for turbulent flow). This analysis was made with the 2.2 kPa *Validyne*™ differential-pressure sensor measurements.

The pressure loss as a function of the water flow was obtained with the oil line closed, operating only with the water centrifugal pump and 7 experimental datasets were recorded. Afterwards, Colebrook's correlation was applied using a commercial steel roughness of 0.046 mm, the pipeline's material. The output was then used in the energy balance equation, resulting in a value of pressure drop. Some discrepancies between the experimental and the calculated data were observed. After a visual inspection of the pipeline's internal surface, it was found that the pipe wall was highly corroded, indicating that the use of the commercial steel pipeline roughness led to an underestimation of the pressure drop.

To estimate the pipeline's actual roughness, an adjustment procedure was performed with Colebrook's correlation and the experimental data collected with water. A roughness value of 0.261 mm—equivalent to that of cast iron—was found, corroborating the findings from the visual inspection (Fig. 2).

The adjustment resulted in a good agreement, as shown at Fig. 3, between the experimental curves and the theoretical ones calculated through the Colebrook's friction-factor correlation.

2.3. Experimental procedure

2.3.1. Oil density and viscosity analysis

Initially, the crude oil behaviour was verified in relation to the dilution with diesel. The best fit for the laboratory data obtained was given by an exponential function. This function was used as a guide for how much diesel would be needed to obtain the desired viscosity to be used in the tests of the experimental line (Fig. 4).

The characterization of the density of the oil and diesel mixtures is useful in calculating the frictional and gravitational pressure gradients (Fig. 5).

The operational-system final data obtained for the oil viscosities and densities can be seen in Table 2-1.

Afterwards, the oil and water phases contact analysis in the pipeline and separation tank began, as emulsion formation was observed. The different velocities of the phases and the shear applied by the pump to the oil-water mixture also contributed to emulsion formation. The importance of studying and characterizing the emulsion formation is that the effective density and viscosity of the emulsion change with watercut.

The watercut was monitored inline by the Roxar WaterCut Meter FullCut. The operational limit of watercut for the experiments was established at 30%. At this point, the emulsion viscosity stood above the pump operational limit, and problems in the flow rate measurement were observed and damage risks were possible.

Water-in-oil emulsions of the four different oil viscosities were produced in the laboratory at varying water proportions and temperatures. The density was measured. The results given by this procedure were compared with the mixture density predicted by the equation originating from Eq. (2.1), where ρ is the density and the subscribed terms stands *e* for emulsion, *o* for oil and *w* for water, presented good agreement with less than 1% error (Fig. 6).

$$\rho_e = \varepsilon_O \rho_O + (1-\varepsilon_O)\rho_W \tag{2.1}$$

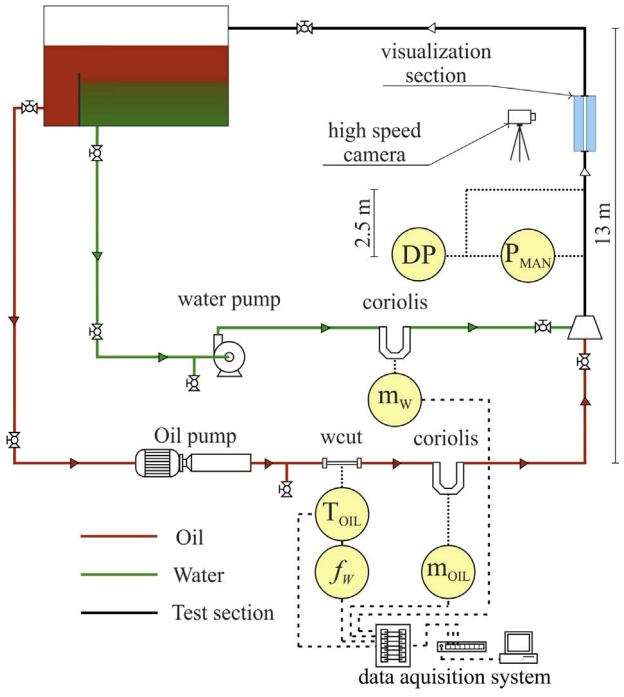

Fig. 1. Diagram of the experimental setup.

Fig. 2. (a) Picture of the pipeline internal surface and (b) a zoom at the extremely corroded area, which results in a higher value for the pipeline roughness.

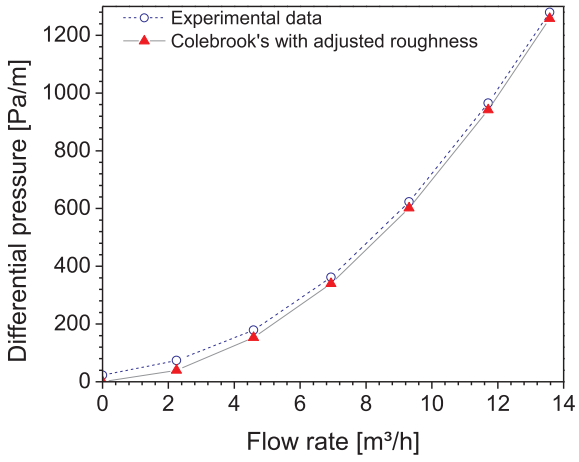

Fig. 3. Experimental and Colebrook's with adjusted roughness data.

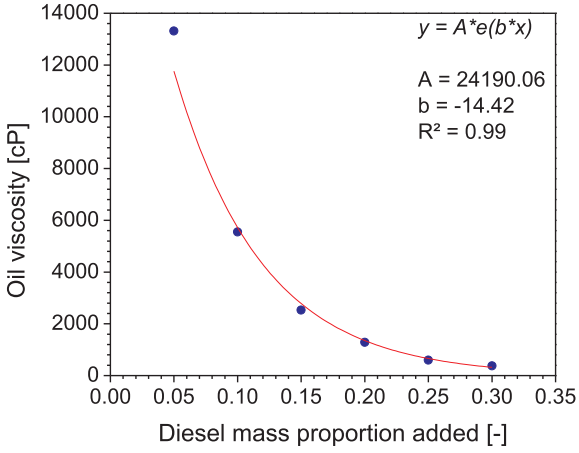

Fig. 4. Viscosity variation as a function of diesel mass proportion added; in red the fit at 25 °C.

$$\rho_e = \rho_O(1-f_W) + \rho_W f_W \quad (2.2)$$

$$\rho_e = [(\rho_O(0°) + aT)*(1-f_W)] + \rho_W f_W \quad (2.3)$$

The same procedure was done for all four oil viscosities used in this work, listed at Table 2-2.

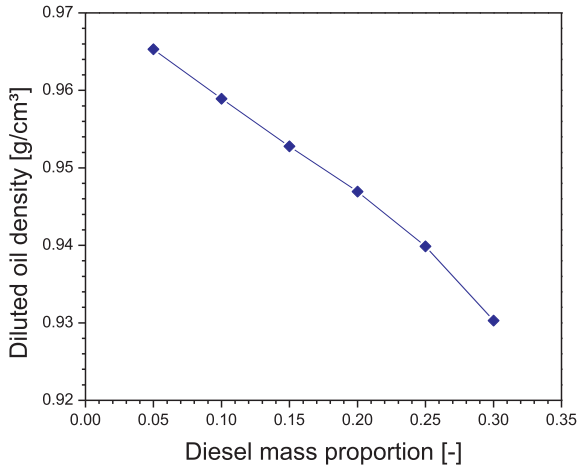

Fig. 5. Oil-diesel mixture density as a function of the diesel mass proportion, at 25 °C.

Table 2-1
Diesel mass quantity needed to reach the required viscosities and its respective densities.

	Desired viscosity [cP]	Measured viscosity [cP]	Measured density [g/cm^3]
Crude oil	34,191	34,191 ± 0.1	0.97031 ± 0.000005
+16.44% diesel	2000	1729 ± 0.1	0.94765 ± 0.00023
+18.35% diesel	1500	1561 ± 0.1	0.94753 ± 0.00001
+21.71% diesel	1000	1112 ± 0.1	0.94352 ± 0.00001
+28.33% diesel	500	557 ± 0.1	0.93688 ± 0.00002

The influence of temperature and watercut to oil viscosity was analysed also. To take that in count, the maximum watercut was monitored inline by the Roxar WaterCut Meter FullCut measurements and a mean between it and the no water oil added to the line was done (Fig. 7).

2.3.2. Experimental routine

First, the crude oil was diluted with diesel to get the viscosity of 1729 cP. The experimental grid was organized in superficial velocities. The experiment started with single-phase water flow. The oil flow was

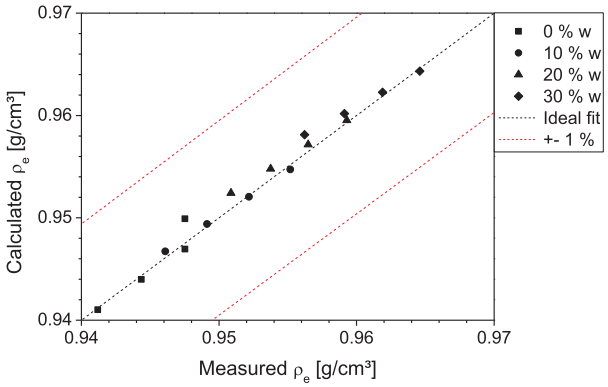

Fig. 6. Experimental and calculated effective oil density for an oil diluted with diesel of 1561 cP for different watercuts.

Table 2-2
Constant values obtained for the density measurements.

Viscosity [cP]	$\rho_o(0°)$ [g/cm^3]	a [g/(cm^3·°C)]
1729	0.96436748	−0.00058906
1561	0.96176495	−0.00059257
1112	0.95899689	−0.00064310
557	0.95277955	−0.00067542

then injected. When steady state was reached, researchers measured the differential pressure and video-recorded the flow for subsequent in-situ volumetric fraction data analysis. The core-annular flow was recorded only for the pair of flow rates above the oil-mixture injection ratio of 50%. Below this, the oil core was unstable and the holdup measurement via image analysis was not possible.

With the first set of tests accomplished, diesel was added to the gravitational separator tank for dilution, yielding the new oil viscosities (1561, 1112 and 557 cP). Prior to commencing a new set of tests for a new viscosity, the watercut was measured. The experimental test grids for all viscosities is presented in Fig. 14, Section 3.1.

2.3.3. Experimental uncertainty

In an experimental study, the uncertainties for the variables directly measured can be estimated by manufacturing a calibration certificate. Other variables derivate from these measurements, and the uncertainties can be estimated performing the uncertainty propagation as presented in Moffat [19]. Considering a function of x statistically independent variables y and z, the uncertainties of x can be represented as,

$$u_x^2 = \left(\frac{\partial x}{\partial y}u_y\right)^2 + \left(\frac{\partial x}{\partial z}u_z\right)^2 \tag{2.4}$$

where u_y and u_z are the standard uncertainties of previously estimated magnitudes of y and z, and u_x is the standard uncertainty propagated on the height x.

Table 2-3 presents the uncertainties directly estimated from calibration certificate.

Table 2-4 presents the propagated uncertainties for the variables presented in this work.

2.4. Flow visualization and image treatment

To measure the in-situ oil volumetric fraction, movies of the core-annular flow were taken with a Redlake Alliance MotionPro X3 high-speed camera, with maximum resolution of 1280 × 1024 pixels. Assembled behind the acrylic display was an illumination system with two fluorescent lamps. The movies were taken at an acquisition rate of 500 fps for two seconds, accumulating 1000 images per pair of flow rates and an image resolution of 7.26 Pixels/mm. The maximum observed velocity was 2 m/s, and the visualization section is 130 mm length, so the flow took 0.06 s to pass through the transparent visualization section, making a frequency of 15 Hz sufficient to analyse the flow. However, considering the Nyquist theorem, the minimum frequency to avoid aliasing is 30 Hz, and the movies were taken at 500 Hz (500 fps), more than sufficient to avoid any problems of data acquisition.

The images were loaded to the software NI Labview™ 2011 from their folder to be processed, Fig. 8(a). The contrast between oil and water phases is enhanced; removing any small oil droplets in the water annulus, Fig. 8(b). One of the RGB colour planes was selected for extraction; the one chosen was proportionated with the most satisfactory results, thus enhancing the image contrast, Fig. 8(c). An image segmentation process was adopted, according to a pre-established threshold that can represent the oil and water phases. Hence, a binary image was obtained, Fig. 8(d). To modify the morphology, researchers applied the function Erode Objects, aiming to prevent a misinterpretation of oil drops at the water annulus as part of the oil core, Fig. 8(e). Then there occurred a pre-defined particle-size removal, providing better interface definition and improving in-situ oil volumetric fraction data analysis, Fig. 8(f). The function Dilate Objects was used, but the dilation had to have the same magnitude as the erosion, which kept the pixels' balance of the oil core once the image erosion modified its pixels across the entire boundary, Fig. 8(g). Finally, if by any means there was a black region inside the oil core, it would be interpreted as a water hole, which is not possible, as observed in the movies; this step filled up those pixels with a unitary value (white), Fig. 8(h).

It is important to note that Remove Small Particles, Fig. 8(f), contributes to relative errors in holdup measurements and consequently data that uses it, propagating the error. The error was taken into account in the uncertainty calculation at Table 2-4.

2.5. Obtaining oil holdup through the images

A matrix of binary data was obtained. The position regarding the oil had a unitary value and the water a value of zero. By summing the pixels along a processed image row, it was possible to acquire the core diameter for that row. Thus the holdup value for that row may be obtained by the ratio of the square core diameter and the square of the sum of pixels one and zero (i.e., the internal diameter of the pipeline). Applying to all the image rows and dividing by the total of rows, it is possible to acquire an average holdup for the image. The in-situ oil volumetric fraction for that footage is obtained by calculating the ratio of all the image holdups and the number of images on the set. It is important to note here that we are considering the flow to be axisymmetric, which is a good approximation for these experiments, according to Rodriguez and Bannwart [20], Bannwart [9] and Oliemans [7]. Fig. 9 presents an example of the image rows sweeping process executed by the algorithm. These data were compared with the predictions of the model proposed by Rodriguez and Bannwart [20] for all four viscosities studied. Fig. 10 shows the time varying holdup values for different oil viscosities studied, with same pair of superficial velocities. With the decrease in oil viscosity, less fluctuation in holdup values is observed and frequency increases. This can be somehow related to the interfacial waves amplitude too.

2.6. Core-annular flow frictional pressure gradient

The main purpose of obtaining the experimental oil holdup is that it is necessary to determine the frictional pressure gradient. For this, considering the *Validyne*™ as the yellow sphere in Fig. 11 and only water entering the pipe and connecting to the instrument, the pressure balance is given by Eq. (2.5).

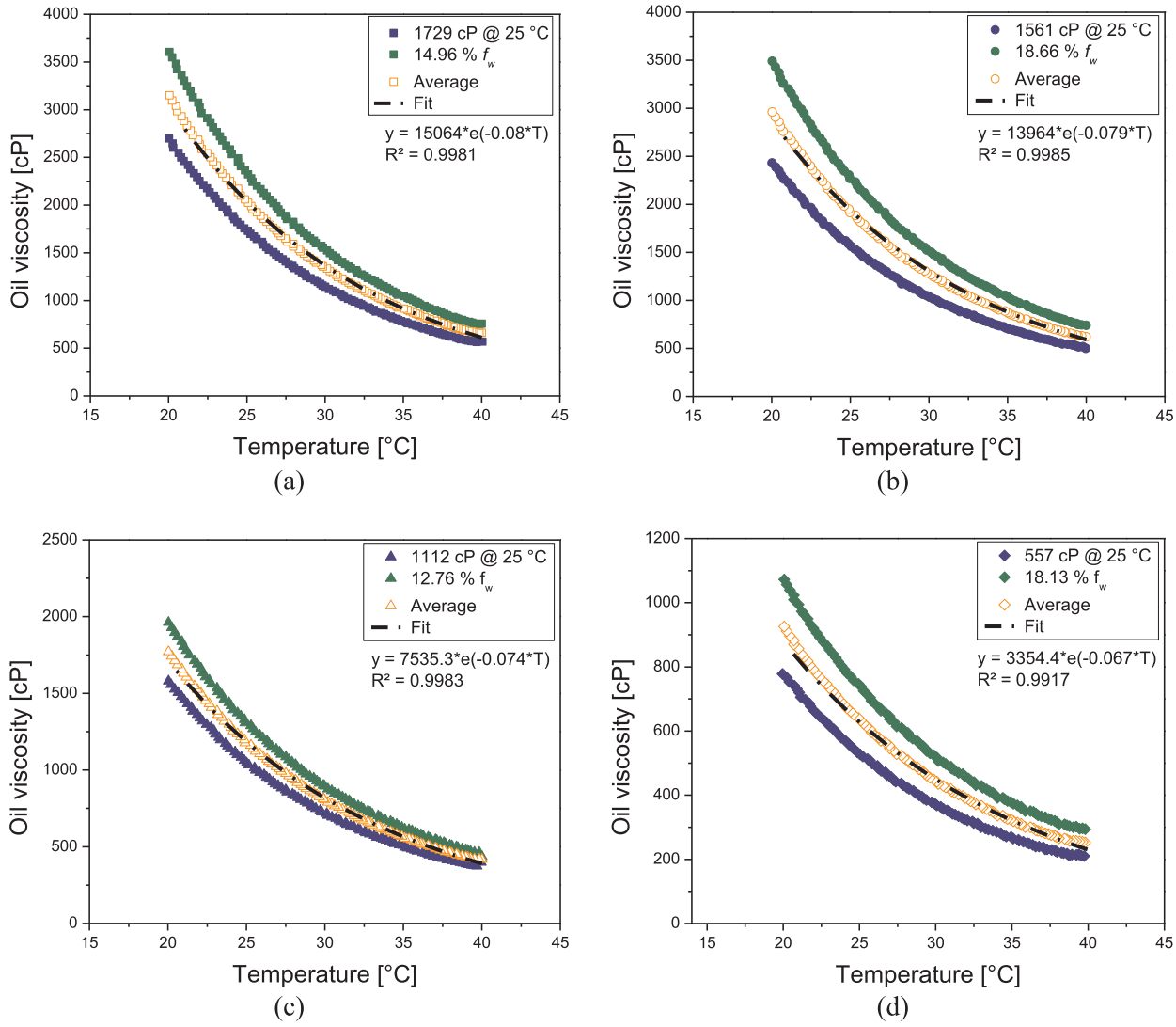

Fig. 7. Minimum, maximum and mean viscosity observed during the experiments, and the fit for 1729 (a), 1561 (b), 1112 (c) and 557 cP (d).

Table 2-3
Uncertainties from calibration certificate for the instrumentation used.

Instrument	Calibration certificate uncertainty
Emerson Micro Motion F series F200 (water Coriolis)	0.2% of the measure
Metroval model RHM40 (oil Coriolis)	0.15% of the measure
Roxar WaterCut Meter FullCut	1.5% of the measure
PT100 temperature sensor	0.75% of the measure
Rosemount model 2088 manometric pressure transducer	0.1% measurement
Validyne™ differential pressure transducer model DP15 with diaphragm #24	0.25% measurement

Table 2-4
Maximum propagated uncertainty values of the measurements obtained in the work, within the experimental conditions.

ρ_W [kg/m^3]	ρ_e [kg/m^3]	J_W [m/s]	J_O [m/s]	ε_O [-]	$\Gamma_{f\ core\ flow}$ [Pa/m]	$\Gamma_{t\ core\ flow}$ [Pa/m]
0.089	2.41	0.1	0.22	0.02373	23.96	1.16

$$P_1 - P_2 = P_1' - P_2' + \rho_W g h \tag{2.5}$$

where P_1 and P_2 are the pressures located at pipeline points 1 and 2, and P_1' and P_2' are the pressures located at the *Validyne*™. The water density, gravity and height between points 1 and 2 are represented by ρ_W, g and h respectively. Now, given that an oil and water mixture is flowing into the pipeline, Eq. (2.6) can be written. By combining Eqs. (2.5) and (2.6) and using the homogeneous model to predict the mixture density, we arrive at Eq. (2.7). The experimental frictional pressure gradient can now be obtained, as seen in Eq. (2.8).

$$P_1 - P_2 = \rho_m g h + \Delta P_f \tag{2.6}$$

$$P_1' - P_2' = (\rho_O - \rho_W) g h \varepsilon_O + \Delta P_f \tag{2.7}$$

$$\Gamma_f = \frac{\Delta P_f}{h} = \frac{P_1' - P_2'}{h} - (\rho_O - \rho_W) g \varepsilon_O \tag{2.8}$$

This shows how important the holdup measurement is to measuring the frictional pressure gradient.

3. Results

3.1. Flow pattern maps

First, prior obtaining the core-annular flow pattern data, a flow

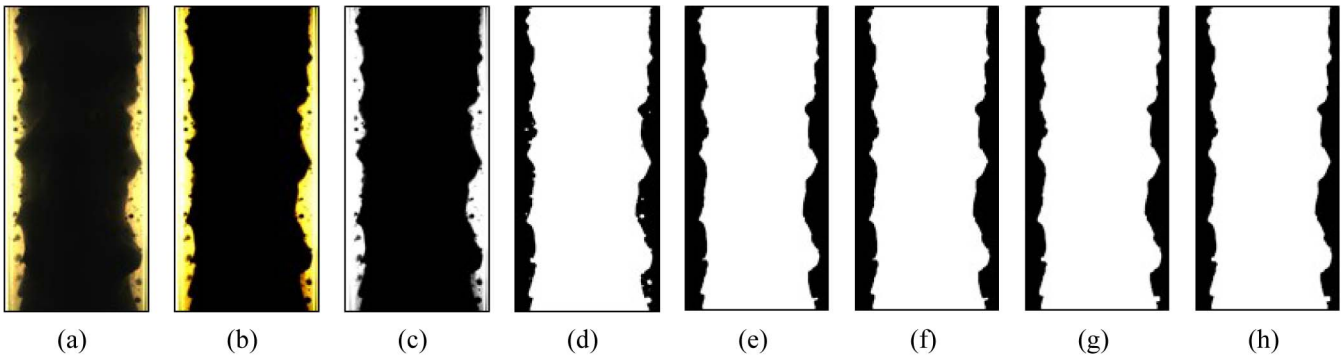

Fig. 8. The sequential treatment of the images, in order from left to right. (a) Load Image; (b) Brightness; (c) Plane Colour Extraction; (d) Threshold; (e) Erode Objects; (f) Remove Small Particles; (g) Dilate Objects; (h) Fill Holes.

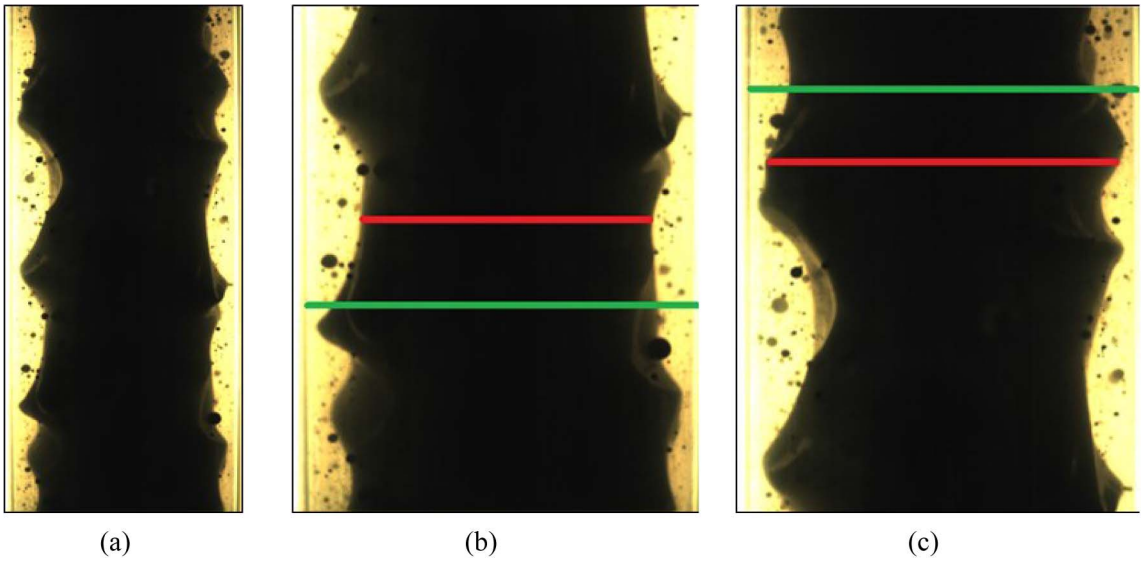

Fig. 9. The whole image (a); a close-up of the process in a thinner core diameter (b); and for a thicker core diameter (c). The green line indicates the internal pipe diameter and the red line the local oil core diameter. 1561 cP oil viscosity. Jw = 0.2 m/s and Jo = 0.6 m/s.

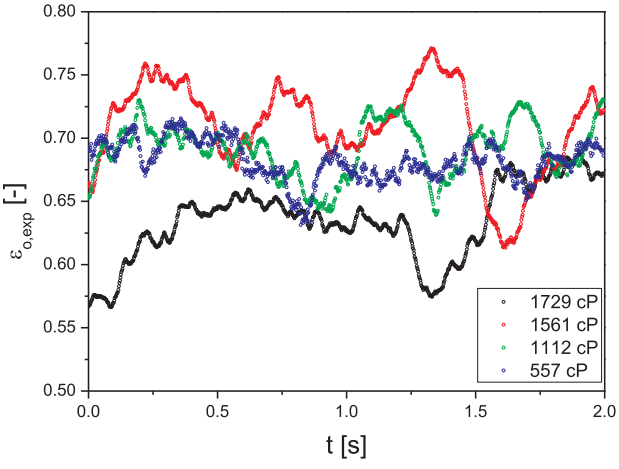

Fig. 10. Time varying holdup values for the four viscosities studied, at the same flow condition of Jw = 0.2 m/s and Jo = 0.6 m/s.

pattern map was taken for each oil viscosity. They can be seen at Fig. 12, where the overlaid points represent a transition between the flow patterns.

It was also taken small footages of the flow patterns identified as Core-Annular Flow (CAF), Intermittent, Bubbles and Dispersed Bubbles, as can be checked at Fig. 13.

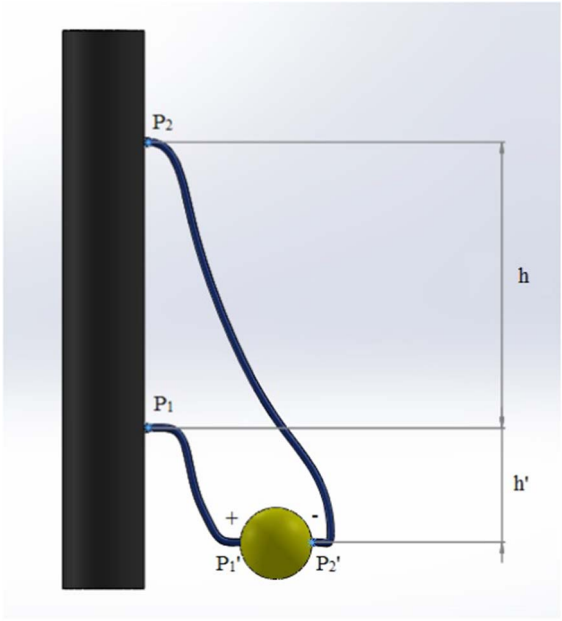

Fig. 11. Scheme of a Validyne™ differential pressure transducer, represented by the yellow sphere.

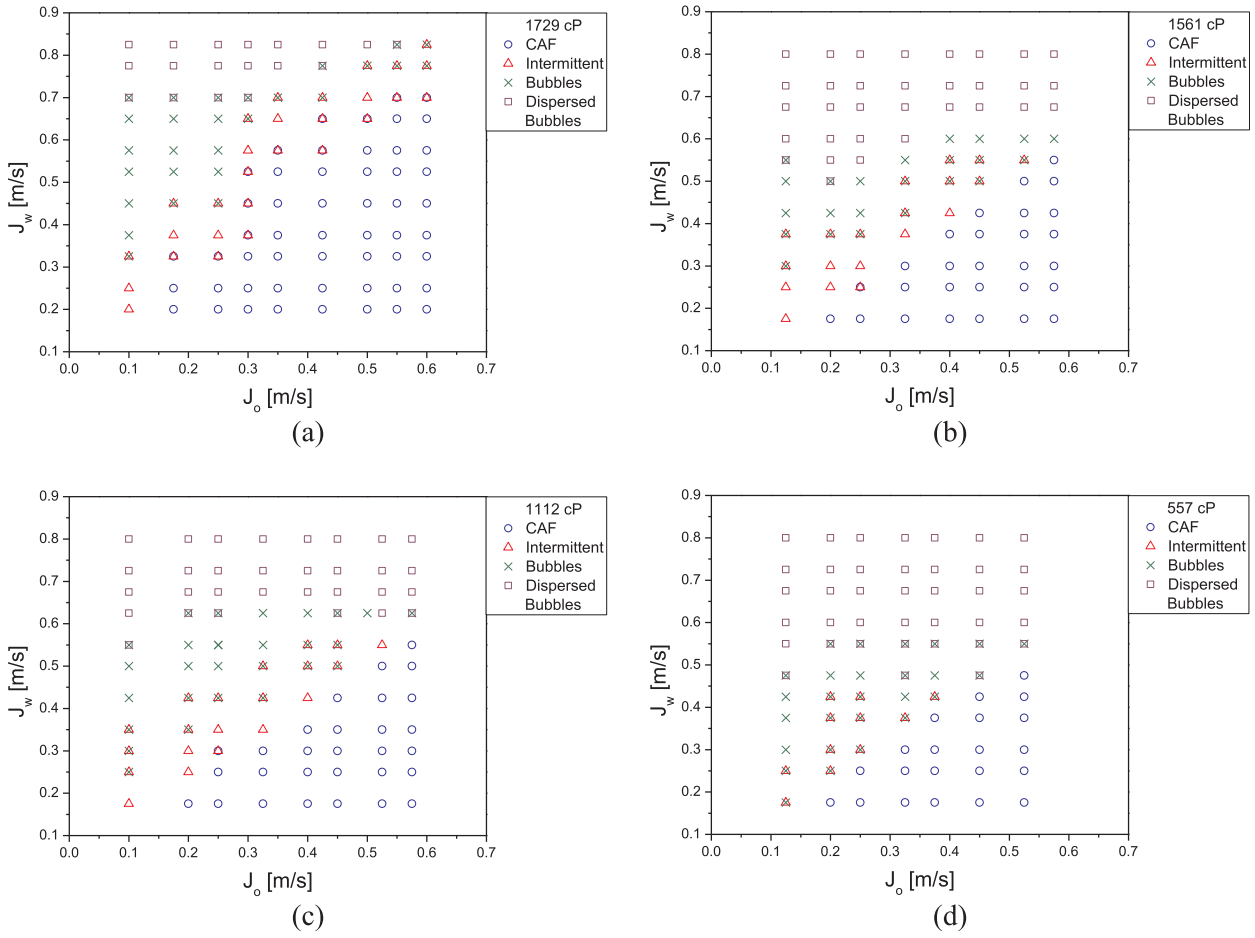

Fig. 12. Experimental system flow pattern maps for oil viscosities of 1729 (a), 1561 (b), 1112 (c) and 557 cP (d).

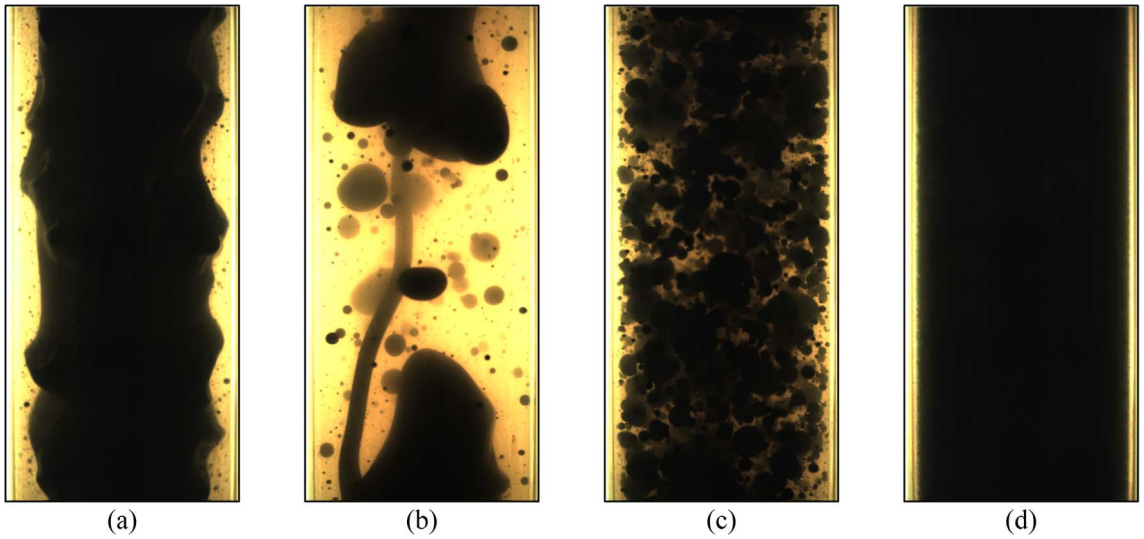

Fig. 13. Flow patterns identified at the present work, Core-Annular Flow (CAF) (a), Intermittent (b), Bubbles (c) and Dispersed Bubbles (d).

It is important to note that there were more experimental points taken, with a maximum water superficial velocity of 0.6 m/s, but for higher values of oil superficial velocity that weren't added to these maps and can be checked at the next section. Moreover, the main difference between Fig. 13(c) and (d) relies on the bubble/droplet size observed, where on oil Dispersed Bubbles flow pattern were much smaller than in oil Bubbles. The oil small bubbles coalescence does not occur because of the high turbulence in the water continuous medium and with their numerous population, turns nearly impossible to visualize through the glass pipe.

3.2. Experimental test grid

Fig. 14 shows the measured points for the four oil viscosities, 1729, 1561, 1112, and 557 cP. The first set of tests for oil at 1729 cP has different increments compared to the other sets of tests for the other

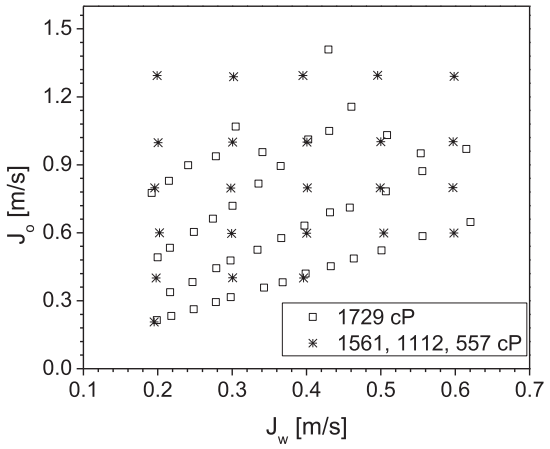

Fig. 14. Experimental test grid (superficial velocities of each phase) for oil at 1729, 1561, 1112, and 557 cP at 25 °C.

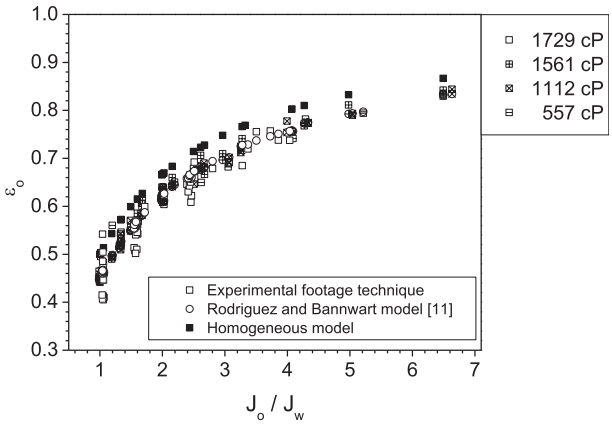

Fig. 15. Experimental in-situ oil volumetric fractions, prediction by the homogeneous model and by Rodriguez and Bannwart model [20] as a function of the ratio of oil and water superficial velocities for all viscosities studied.

Table 3-1
Holdup average relative error between experimental footage technique and the homogeneous model, for the four viscosities studied in the present work.

Viscosity [cP]	1729	1561	1112	557
ARE [%]	12.56	6.06	7.40	6.80

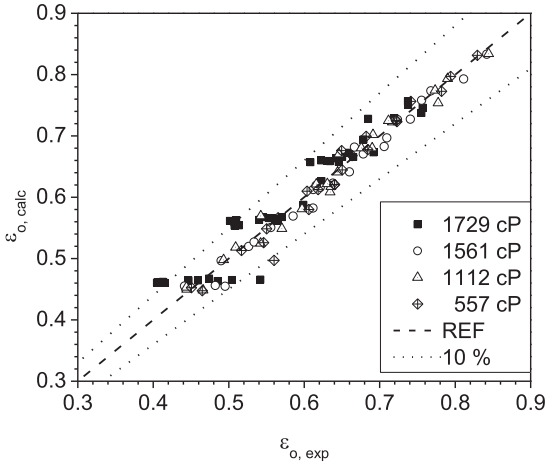

Fig. 16. Comparison of oil holdup between the experimental footage technique and Rodriguez and Bannwart model [20], for all viscosities studied.

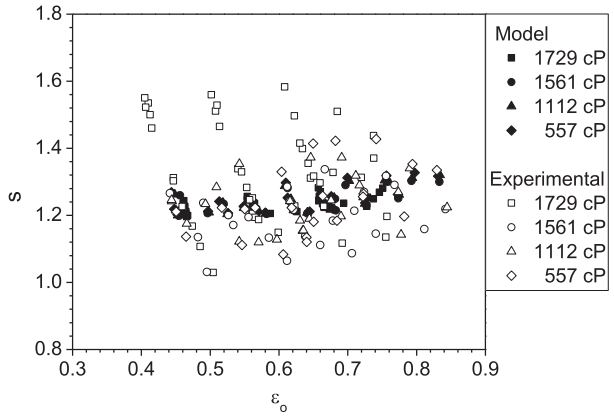

Fig. 17. Slip ratio between the phases, experimental data and Rodriguez and Bannwart model [20], as a function of oil holdup for the studied viscosities.

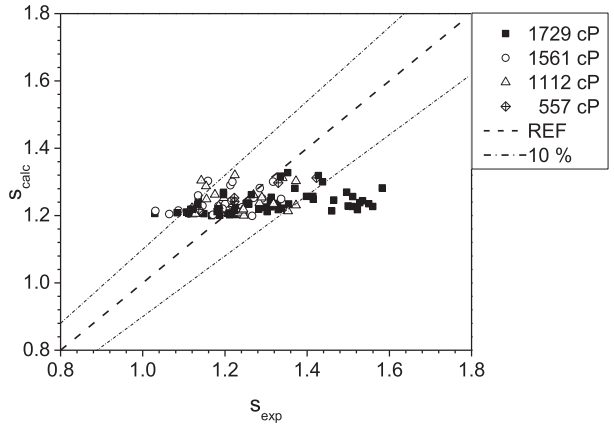

Fig. 18. Comparison between the experimental and calculated slip.

viscosities. This is because the first set of experiments were at the operational limits of the system, used for mapping the possible operational range of the setup.

3.3. Oil holdup and slip ratio analysis

The values of oil holdup obtained by processing the images were in good accordance with values reported in the literature, Rodriguez [11], with a maximum error of 26% and almost all the results below 10%, for all viscosities. When core-annular flow pattern exists, the observed slip ratio above unity means a higher oil-core real velocity. It leads to smaller oil in-situ volumetric fractions than those predicted by the homogeneous model. Fig. 15 shows, as a function of the ratio of oil and water superficial velocities, the oil-holdup data obtained with the footage technique, predictions of the homogeneous model, as well as the model of Rodriguez and Bannwart [20]. Higher values for the homogeneous model were expected, as it does not count the presence of the slip between the oil and water phases.

Table 3-1 shows the average relative error (ARE) between the experimental footage technique and the homogeneous model, for all four viscosities.

Fig. 16 compares the model of Rodriguez and Bannwart [20] ($\varepsilon_{o,calc}$) and the experimental footage technique ($\varepsilon_{o,exp}$). The dashed line represents the optimum agreement between the model and experimental data.

Most of the discrepancies of the data of Fig. 16 were less than 10%. Almost all the higher differences were for low oil superficial velocities, where the oil core was unstable, which increases the uncertainty of the footage technique.

The experimental data and Rodriguez and Bannwart model [20]

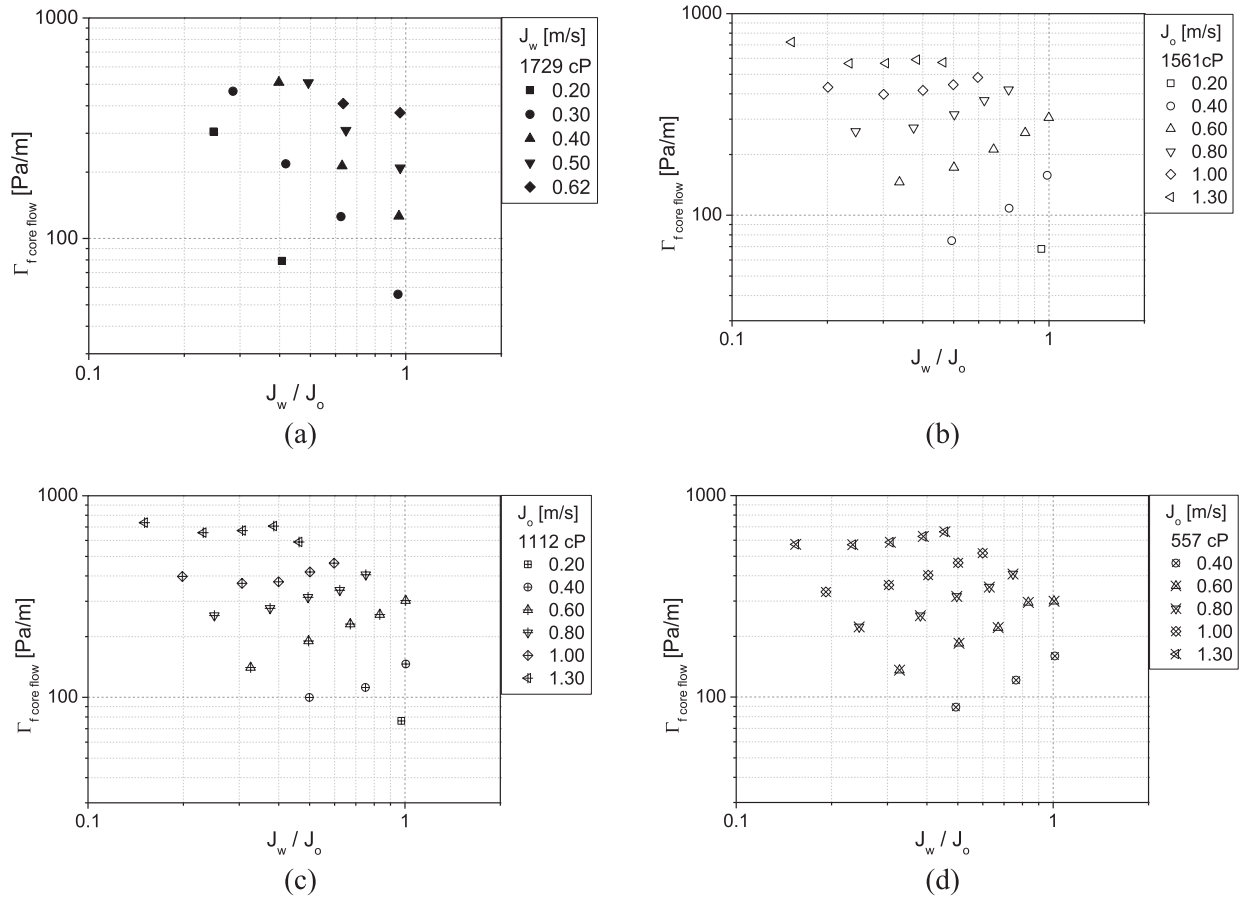

Fig. 19. Frictional pressure gradient for the oil at 1729 (a), 1561 (b), 1112 (c), and 557 cP (d) as a function of the ratio of water and oil superficial velocities for different oil superficial velocities.

predictions for the slip ratio can be checked in Fig. 17. It can be observed that the slip ratio always stands above the unity, which means the oil real velocity was always higher than the water real velocity. Also, the experimental data presented higher slip-ratio values than those predicted by the Rodriguez and Bannwart model [20].

A close analysis of Fig. 17 shows that the slip-ratio range of the experimental data are wider than that calculated by the model. Furthermore, a comparison of the slip ratios amongst the four different viscosities studied assumes higher values as oil viscosity increases, which is not observed in the calculated data. While the experimental slip ratio ranges between 1.04 and 1.60, the model predictions range between 1.08 and 1.44.

A high density of solid black squares is present outside the ± 10% dashed lines in Fig. 18, corresponding to the higher viscosity of 1729 cP. A look back to Fig. 17 helps explain this. Here, a relationship is visible between the slip ratio and the oil viscosity: the slip ratio decreased as the oil was diluted with diesel. Although the Rodriguez and Bannwart model [20] shows good results for holdup and slip ratio predictions, its parameters were fitted for the condition of 500 cP oil viscosity, which can have a significant impact on the prediction for other viscosities, as shown in Fig. 18.

3.4. Frictional pressure gradient in core-annular flow

As noted above, the frictional pressure gradient in core-annular flow is expected to assume lower values than oil single-phase flow. This is due to the water film in the annulus, preventing the viscous oil from coming in contact with the pipe wall. For a fixed oil superficial velocity, the amount of water in the film affects the frictional pressure gradient, resulting in an ideal water flowrate for each oil flowrate, as can be seen in Fig. 19. For the four viscosities shown, it may be observed that with the increase of the oil superficial velocity, less water is needed to reach the minimum frictional pressure gradient (the minimum point tends to move to the left as the oil flow rate rises). This observation has already been made by Joseph et al. [13] and Rodriguez and Bannwart [11]. Furthermore, one may notice that the frictional pressure gradient stands almost the same for the viscosities studied in Fig. 19 (1729, 1561, 1112, and 557 cP).

This data reflects the lubrication effect pursued by the flow pattern studied, whereas the oil viscosity does not really affect the frictional pressure gradient because there is no contact with the pipe wall. In the end, the frictional pressure gradient almost solely depends on the annulus fluid viscosity – water in this work.

For the viscosity of 1729 cP, a different approach was used, one where the water flowrate was maintained as constant and the oil flowrate changed. As the oil flow rate changed, it was very difficult to keep the water flow rate steady.

3.5. Comparison of frictional pressure gradient in single-phase oil flow and core-annular flow

Presented in Fig. 20 is the reduction factor—the ratio between the frictional pressure gradient of single-phase oil flow and core-annular flow. The friction factor was calculated using Colebrook's correlation and the same oil superficial velocity corresponding to the core-annular flow was used. This comparison allows researchers to check the core-annular flow pattern energetic efficiency compared to single-phase oil flow. The reduction factor decreased with the oil dilution, as expected, because the less viscous oil flows more easily, with less friction between the oil and the pipe wall.

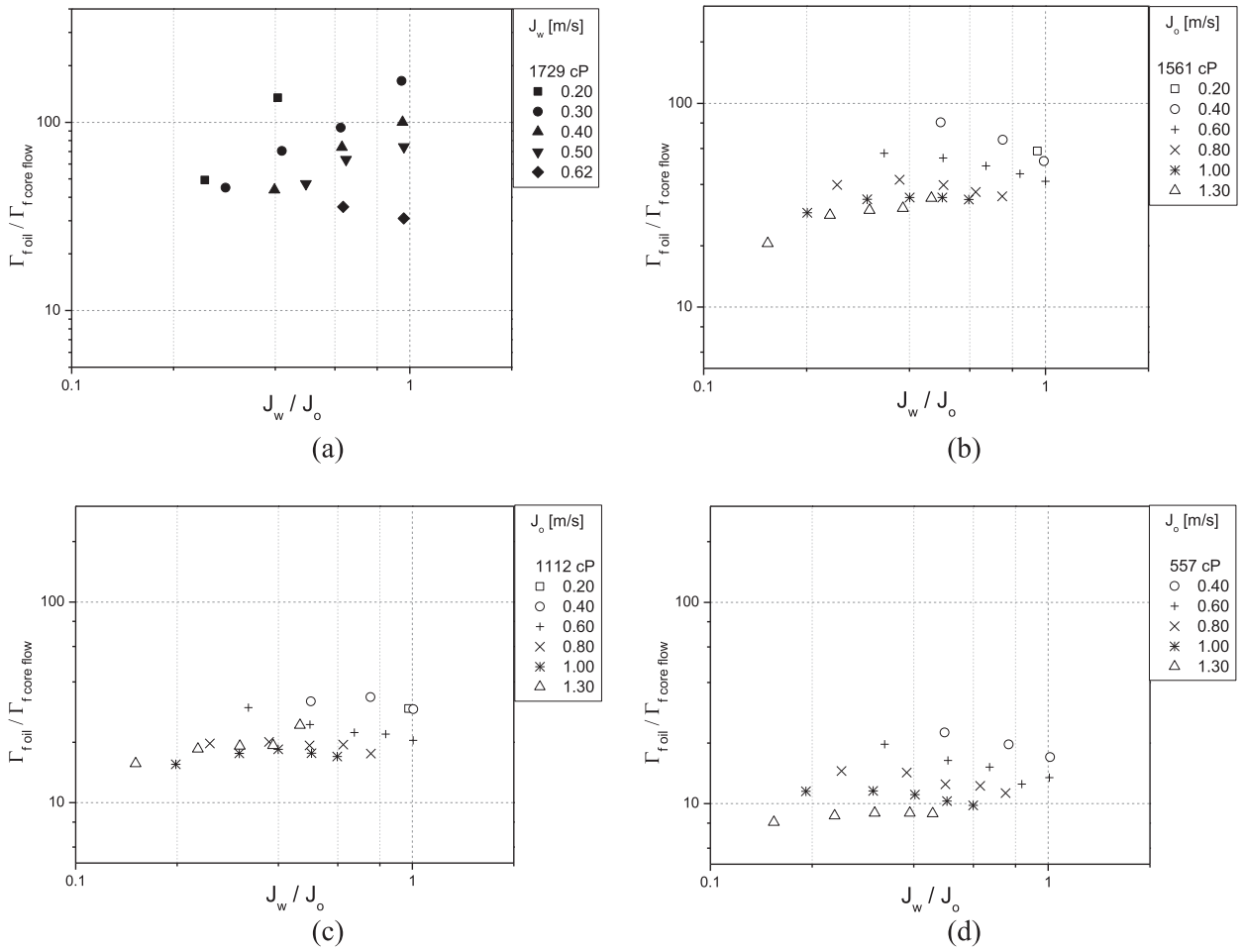

Fig. 20. Comparison between the frictional pressure gradient of single-phase oil flow and the obtained experimentally for the core-annular flow, for the viscosities of 1729 (a), 1561 (b), 1112 (c), and 557 cP (d).

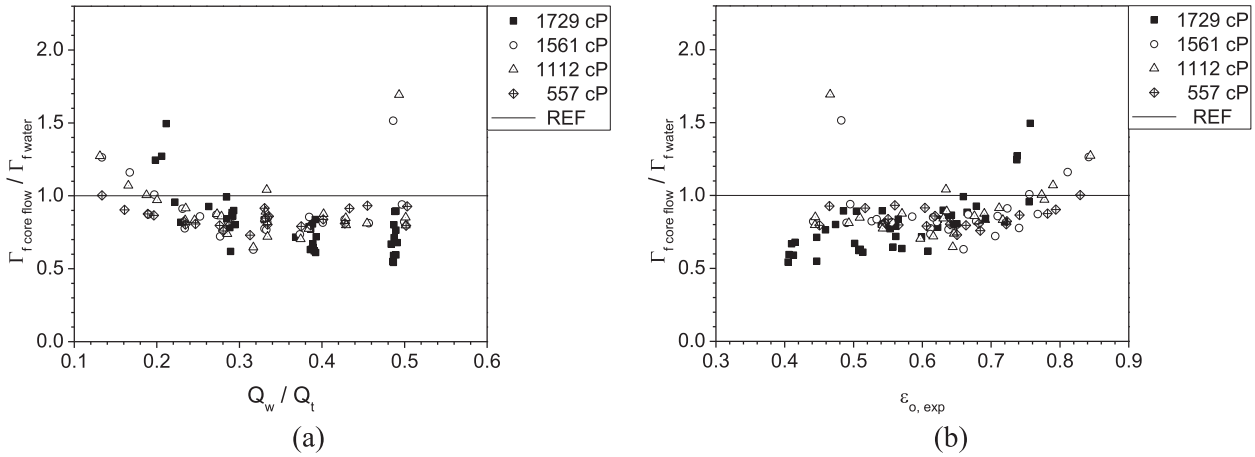

Fig. 21. Ratio of frictional pressure gradient of core-annular flow and single-phase water flow, with experimental holdup acquired for all viscosities, as a function of the water input ratio (a) and of the experimental oil holdup (b).

As can be seen in Fig. 20, for the viscosities of 1729 and 1561 cP, the reduction factor reached values of up to 100, whereas for the lower viscosities of 1112 and 557 cP it reached values of up to 40. This exemplifies the potential benefit of using the core-annular flow in production and/or transport of viscous oils. The significant reduction in the frictional pressure gradient results in less energy needed for the process.

3.6. Comparison of frictional pressure gradient in single-phase water flow and core-annular flow

Fig. 21 shows the ratio between the core-annular flow frictional pressure gradient ($\Gamma_{fcore\text{-}flow}$) and the corresponding single-phase water flow at the same total volumetric flow rate ($\Gamma_{f\ water}$). The ratio of frictional pressure gradients is presented as a function of the water input ratio and oil holdup. The data shown uses the oil holdup taken from the

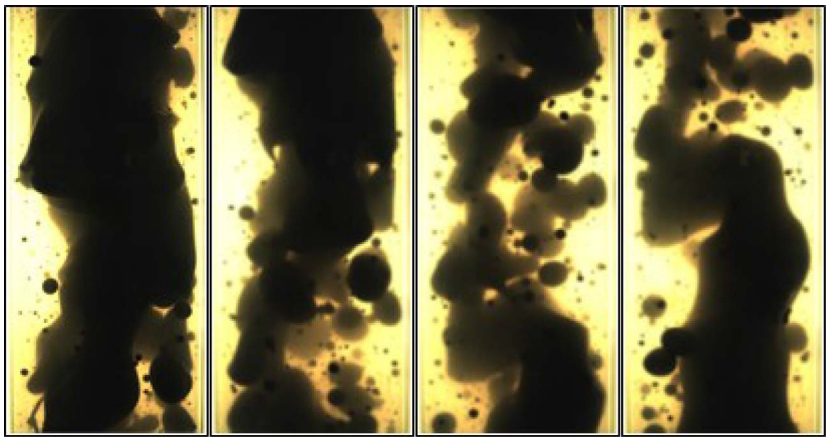

Fig. 22. Sequence of images at 1561 cP oil viscosity but the same experimental conditions. Evolution of upward-vertical flow from left to right, the time increment between displayed images is 0.1 s (Jw = 0.19 m/s and Jo = 0.20 m/s).

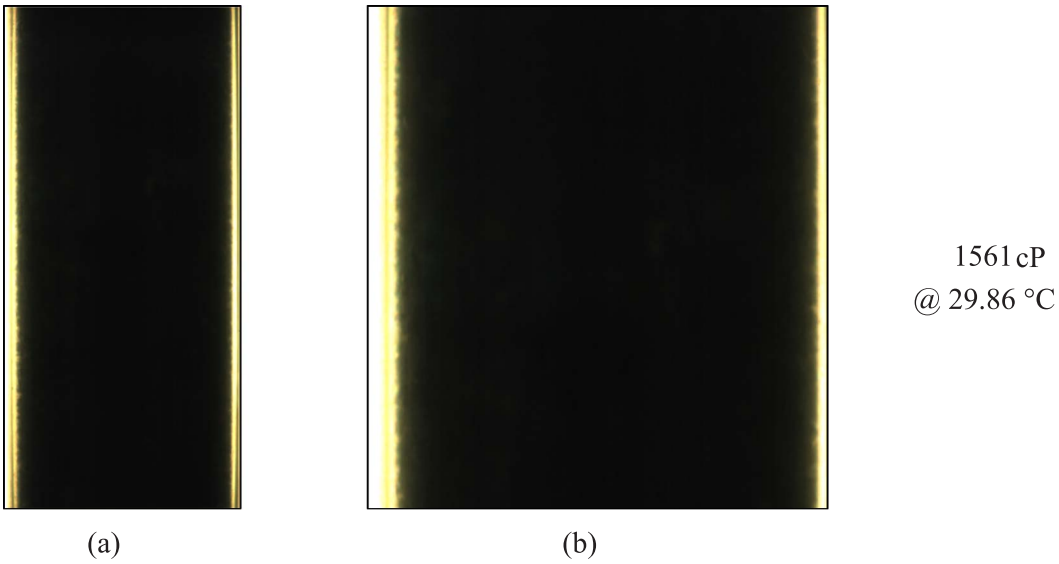

Fig. 23. (a) the whole image; (b) a zoom of the same image. A very thin film of water is present at this pair of superficial velocities (Jw = 0.19 m/s and Jo = 1.30 m/s).

image treatment.

As might be expected given findings from the literature [11,13], the ratio between these frictional pressure gradients stood, for the most part, below the unity. The points below the unity indicate flows in which the frictional pressure gradient of the oil-water mixture was lower than that of the single-phase water flow. Already reported in the literature, the finding is corroborated here [11,13].

It can be observed in Fig. 21(a) that for water input ratios below 0.2 the ratio becomes greater than the unity. The small amount of water builds into a very thin film of water, so the flow pattern is not stable and the frictional pressure gradient increases, as the water film tends to break and the oil core come in contact with the pipe wall. Besides that, the great interfacial shear stress between the phases caused by high oil flow rate results in higher frictional pressure gradients too. Water input ratios between 0.2 and 0.5 are related to the smallest frictional pressure gradient ratios, always below the unity.

In the case of water input ratios above 0.5, ratios above the unity can be observed. Because the amount of oil injected is low, the oil core starts to become unstable. The beginning of flow-pattern transition to intermittent flow was observed. This was characterized by very long interfacial waves, with oil-core ruptures. The oil-core rupture increases frictional losses in the flow leading to a higher frictional pressure gradient.

According to Bannwart et al. [21] the condition for the existence of core-annular flow is oil holdups of higher than 0.5. To analyse this, the same data of frictional pressure-gradient ratio of Fig. 21(a) was plotted using oil holdup as abscissa; see Fig. 21(b). Fig. 21(b) shows that for oil holdups higher than 0.75, the frictional pressure-gradient ratio starts to increase. This is caused by, as explained above, the water breaking the oil core into droplets, which then come in contact with the pipe wall. Further increments in the oil holdup change the flow to an almost single-phase oil flow, increasing the frictional pressure gradient by a great deal. The opposite occurs for oil holdups below 0.45. Here, the water flow destabilizes the oil core leading the flow-pattern to transition to an intermittent flow, which increases the frictional pressure gradient due to the intense momentum transfer between the phases.

Moreover, it was noticed that, as the oil viscosity decreased, the stable region where the core-annular flow pattern was observed moved towards higher values of oil superficial velocities. Fig. 22 shows a sequence of images under the same experimental conditions for a sample of 1561 cP oil. In Fig. 22, an unstable core-annular flow pattern can be seen. This is the case for the low oil holdup. In this sequence of images, one can observe the lack of a stable oil core: the oil flows as a core sometimes, but in a water-continuous medium it can be replaced by oil drops, and then the oil core can return, though measuring the oil holdup via high speed camera in such a flow condition is not possible. A case of high oil holdup is shown in Fig. 23. Only a small and thin film of water is present, already being incorporated into the oil core. This permits the oil to easily reach the pipe wall and thus increase the frictional pressure gradient. For the higher viscosity of 1729 cP, the operational pumping limit was exceeded by such oil superficial velocity (the pump could not manage it).

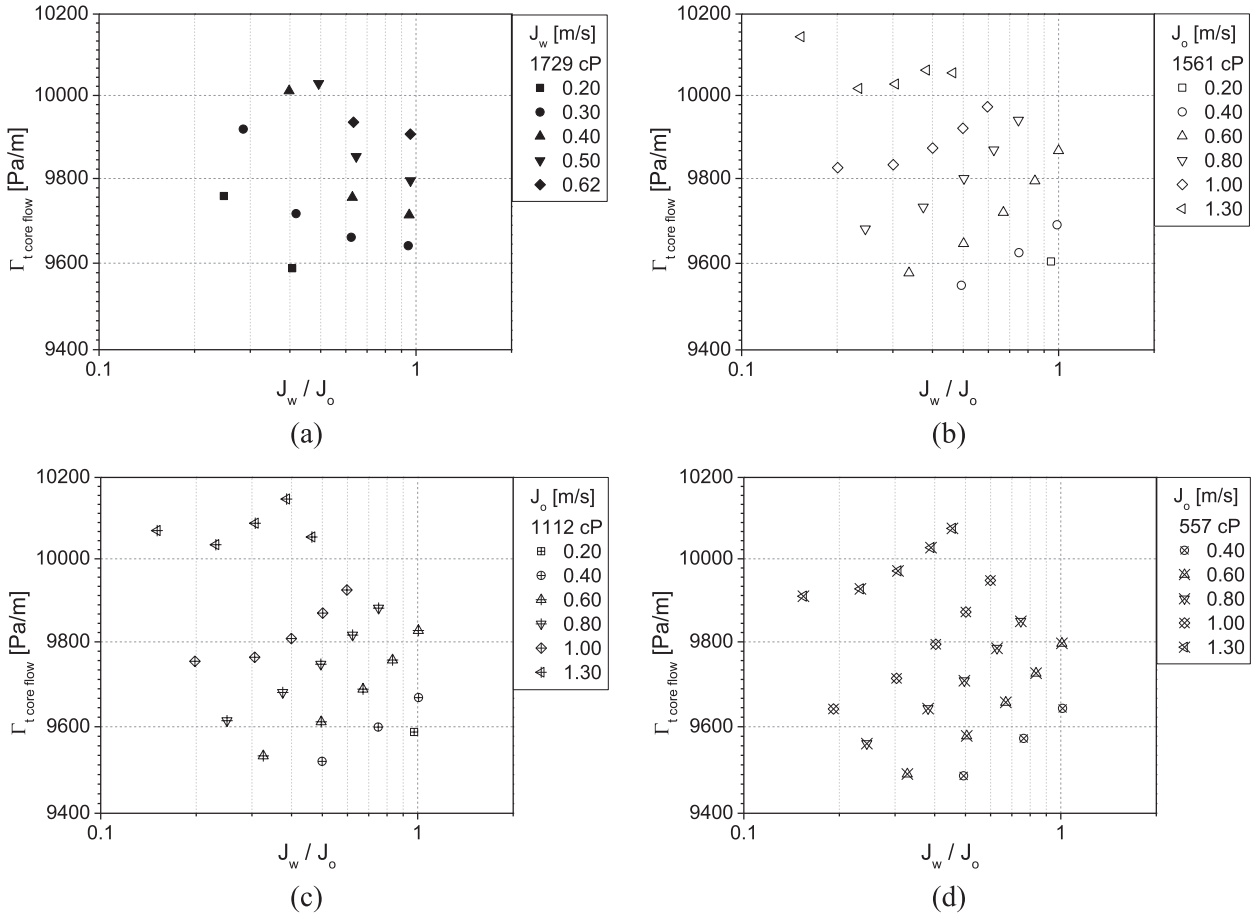

Fig. 24. Total pressure gradient for the core-annular flow with the oil at 1729, 1561, 1112, and 557 cP as a function of the water input ratio for different oil superficial velocities.

3.7. Total pressure gradient and reduction factor in core-annular flow

The total pressure-gradient value in upward vertical flow consists in the sum of two shares—the frictional and the gravitational pressure gradients. As there is no phase change, the fluids are incompressible and no change in the pipe cross-sectional area is observed, the accelerational pressure gradient can be neglected. The real pressure drop is shown, thereby implying the energy necessary to transport a fluid through the pipe. With the total pressure-gradient reduction factor, the efficiency related to the core-annular flow as an artificial lift method can be evaluated in relation to the single-phase oil flow in a pipeline. The single-phase oil flow calculations were done using Colebrook's friction factor. The total pressure gradient stood around the same values for all the viscosities, at the range of 9.4 to 10.2 kPa/m, as shown in Fig. 24.

The total reduction factor for all the viscosities studied can be observed in Fig. 25. It varied from a maximum value of 3.36 for 1729 cP viscosity to a minimum value of 1.24 for 557 cP. A comparison of the data in Fig. 25 reveals that with a decrease in oil viscosity by adding diesel, a decrease is brought about in the total reduction factor. Furthermore, it can be observed that by increasing the oil superficial velocity, there is an increase in the reduction factor. This can be explained by analysing the portions related to the frictional and gravitational pressure gradients simultaneously; in single-phase oil flow, an increase in the oil superficial velocity implies an increase in the frictional pressure gradient, while the gravitational portion does not change. In core-annular flow, increasing the oil superficial velocity results in a reduction in the gravitational pressure gradient and in a slight increase in the frictional pressure gradient (of the same order of water single-phase flow).

3.8. Viscosity influence on flow parameters

This section aims to shed light on whether and if so how the core-annular flow parameters are affected by the crude oil dilution with diesel. Some important two-phase flow parameters such as frictional and total pressure gradients, slip ratio, holdup and total reduction factor are shown in Tables 3-2–3-4. These are the data for a fixed oil superficial velocity of 0.8 m/s and three different water superficial velocities of 0.2, 0.4, and 0.6 m/s. Such oil superficial velocity was unattainable for the viscosity of 1729 cP, so these data are not presented. Additionally, the recorded images of each experiment are shown, permitting the checking for similarities and for qualitatively observation purposes.

Table 3-2 and Fig. 26 present the data for the different viscosities of the lowest water superficial velocity. It can be observed that the most stable core, as expected, is the one related to 1561 cP and as the viscosity decreases, the flow pattern starts to present drops in the annulus, leading to higher momentum transfer between the phases and higher pressure drop. With a decrease in viscosity, there is observed a slight decrease of the frictional pressure drop, though almost no difference in the total pressure gradient. Finally, the reduction factor decreases as the viscosity decreases due to the increase in the momentum transfer.

The conclusions made concerning the data presented in Table 3-2 and Fig. 26 can be made again for the data in Table 3-3 and Fig. 27. The only noticeable difference is that the increase in the water superficial velocity causes an increase in the water-annulus thickness, increasing the momentum transfer and the amount of oil drops inside the annulus.

In Table 3-4 and Fig. 28, in the 1112 cP case, the increase in the water superficial velocity completely destabilizes the oil core. In addition, for the core-annular flow related to the 1561 cP oil viscosity there

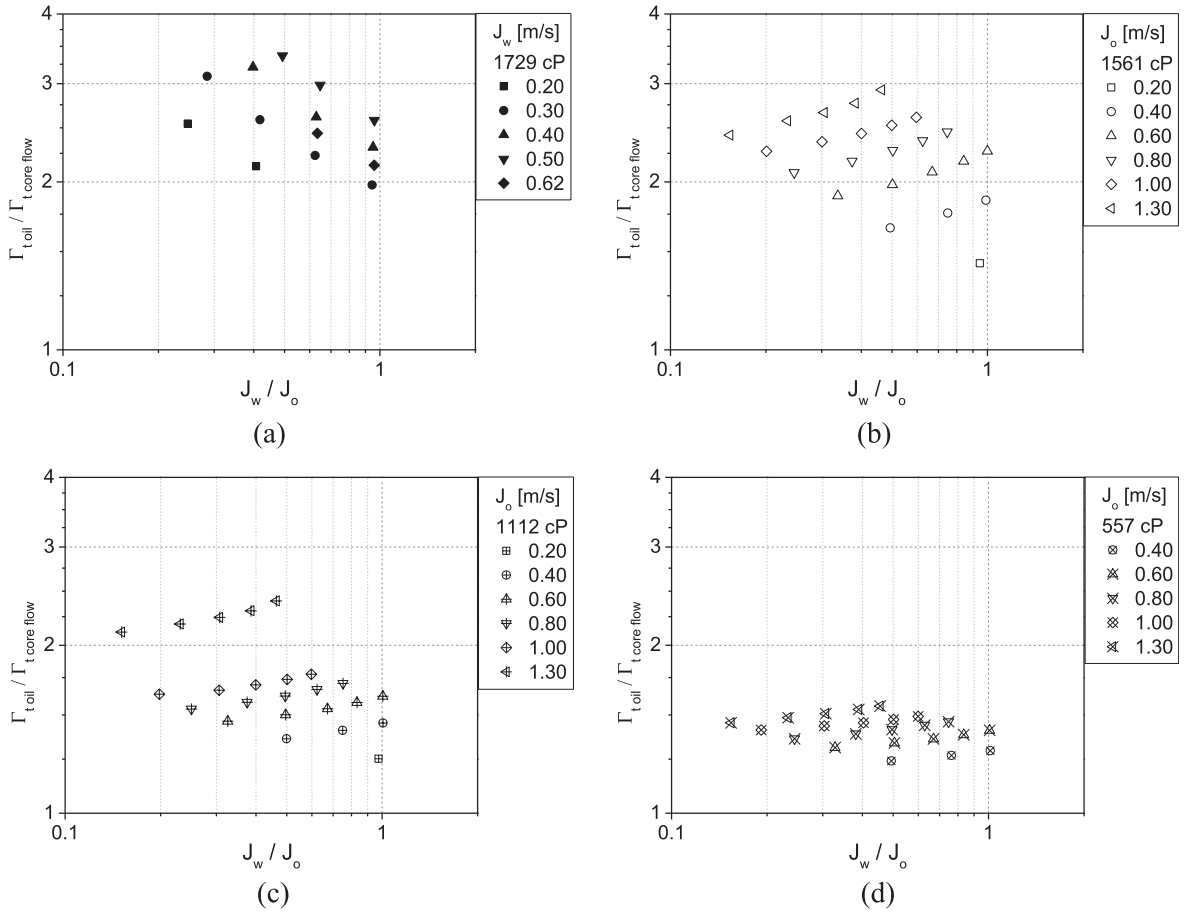

Fig. 25. Total pressure gradient Reduction Factor for the oil at 1729 (a), 1561 (b), 1112 (c), and 557 cP (d) as a function of the injection ratio of water and oil for different oil superficial velocities.

Table 3-2
Two-phase flow parameters for three different oil viscosities at oil and water superficial velocities of 0.8 and 0.2 m/s, respectively.

J_o = 0.8 and J_w = 0.2 m/s					
μ_o [cP]	Γ_f [Pa/m]	Γ_t [Pa/m]	$\varepsilon_{o,exp}$ –	s_{exp} –	$\Gamma_{t\ oil}/\Gamma_{t\ core-flow}$ –
1561	260.652	9680.776	0.756	1.317	2.315
1112	254.373	9614.087	0.778	1.142	1.603
557	222.884	9560.559	0.741	1.427	1.744

Table 3-3
Two phase flow data parameters for three different oil viscosities at oil and water superficial velocities of 0.8 and 0.4 m/s, respectively.

J_o = 0.8 and J_w = 0.4 m/s					
μ_o [cP]	Γ_f [Pa/m]	Γ_t [Pa/m]	$\varepsilon_{o,exp}$ –	s_{exp} –	$\Gamma_{toil}/\Gamma_{t\ core-flow}$ –
1561	316.377	9800.057	0.616	1.242	2.561
1112	313.848	9746.772	0.631	1.185	1.701
557	332.530	9708.050	0.640	1.134	1.875

is a greater amount of oil droplets, but the larger thickness of the annulus lead to a higher reduction factor.

The effect in the reduction factor due to the viscosity is presented in Fig. 29, where an exponential increase of the factor is observed as the viscosity increases for all water superficial velocities. This confirms the best result of core-annular flow as the oil becomes more viscous.

Table 3-4
Two phase flow data parameters for three different oil viscosities at oil and water superficial velocities of 0.8 and 0.6 m/s, respectively.

J_o = 0.8 and J_w = 0.6 m/s					
μ_o [cP]	Γ_f [Pa/m]	Γ_t [Pa/m]	$\varepsilon_{o,exp}$ –	s_{exp} –	$\Gamma_{t\ oil}/\Gamma_{t\ core-flow}$ –
1561	420.077	9940.099	0.534	1.171	2.784
1112	405.877	9880.853	0.542	1.122	1.802
557	408.218	9849.355	0.546	1.112	1.992

4. Conclusions

An analysis of frictional pressure-gradient data reveals the core-annular flow pattern to be an attractive technique for artificial lift and for transporting high-viscous oils. In this experimental study, a crude oil was used, diluted with diesel at four different viscosities (1729, 1561, 1112 and 557 cP). The measured frictional pressure gradient had the same magnitude of water single-phase flow at the mixture flow rate.

This study showed the Rodriguez and Bannwart model [20] to be robust at predicting the oil holdup and slip ratio between the phases for the core-annular flow pattern. There was good agreement with the experimental data and with no significant changes in the oil holdup values due to the oil dilution with diesel. Some of the slip-ratio experimental data for the 1729 cP viscosity were beyond the 10% point spread, suggesting an investigation into the relation between slip-ratio and oil viscosity should be done.

The flow footage technique and image treatment for obtaining the oil holdup was shown to be practical, although still necessary are a

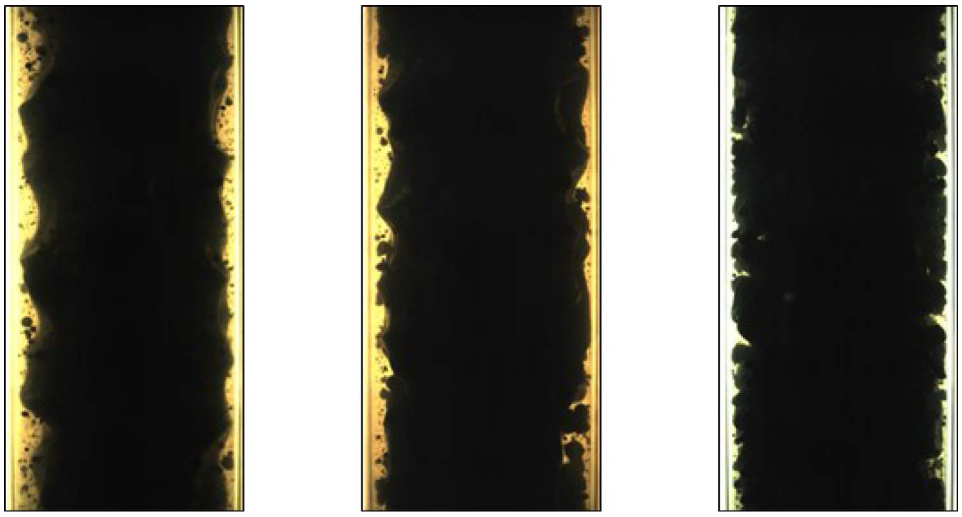

(a) @1561 cP and 29.27 °C (b) @1112 cP and 33.87 °C (c) @557 cP and 31.04 °C

Fig. 26. Two-phase flow images for the three different oil viscosities listed on Table 3-2 at oil and water superficial velocities of 0.8 and 0.2 m/s, respectively.

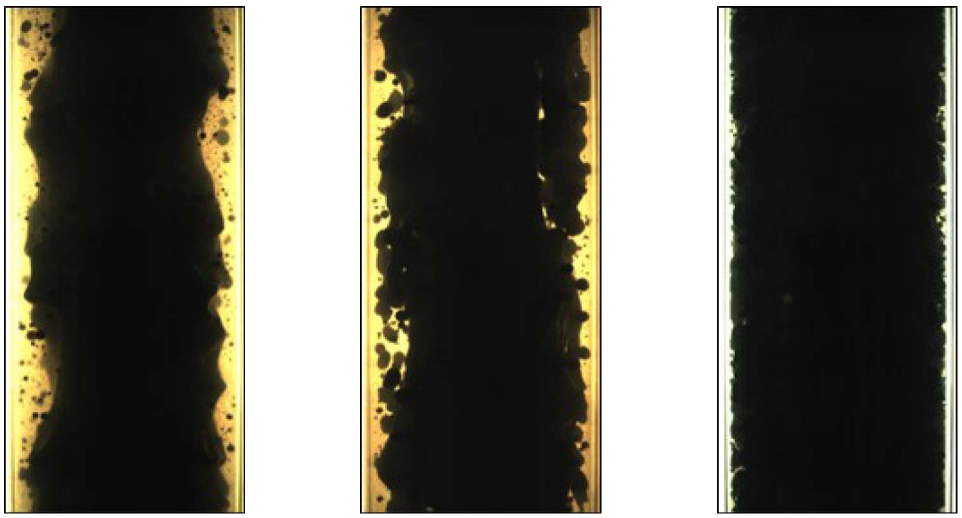

(a) @1561 cP and 29.20 °C (b) @1112 cP and 33.77 °C (c) @557 cP and 30.92 °C

Fig. 27. Two phase flow images for three different oil viscosities listed on Table 3-3 at oil and water superficial velocities of 0.8 and 0.4 m/s, respectively.

priori knowledge of the flow pattern and a good threshold value judgment by the operator. Nevertheless, further research of the errors this image treatment algorithm might imply on oil holdup should be held.

By visualizing the flow, it was verified that the minimum oil holdup for a stable core-annular flow increases with a decrease in the oil viscosity, i.e., they are inversely proportional. In other words, the transition boundary for core-annular flow pattern is located at higher oil superficial velocities, taking into count a fixed water superficial velocity. This might be explained by the requirement of more oil to preserve the oil core, compensating for the lower interfacial tension because of the presence of more diesel. Consequently, it is easier for the oil core to be torn apart. In addition, the dilution with diesel decreases the oil-diesel mixture density, resulting in higher values of buoyancy, promoting higher detachment of oil droplets.

The core-annular frictional pressure gradients were of the same magnitude as those of single-phase water flow at the mixture flow rate. In some cases, the gradient was even smaller than that of single-phase water flow. Compared with single-phase oil flow, frictional reduction factors of up to 100 times were observed for the maximum viscosity studied (1729 cP). The total pressure gradient (gravitational + frictional) in core-annular flow was smaller than that of single-phase oil flow. Compared to single-phase oil flow, total reduction factors of up to 4 times were observed.

An analysis of the viscosity influence on flow parameters has been presented, although an interfacial tension analysis would give a leaner analysis. For the pairs of superficial velocities studied, the viscosity decrease didn't change or lead to a slight decrease in frictional pressure drop and almost no difference in the total pressure gradient. It was observed that a thicker water annulus led to higher reduction factors. The core-annular flow reduction factor presents an exponential increase with the increase of the oil viscosity for all water superficial velocities.

Acknowledgments

The authors are grateful to CAPES (Comissão de Aperfeiçoamento de Pessoal do Nível Superior) for Caio's grant, Petrobras/CENPES and ANP "Compromisso de Investimentos com Pesquisa e

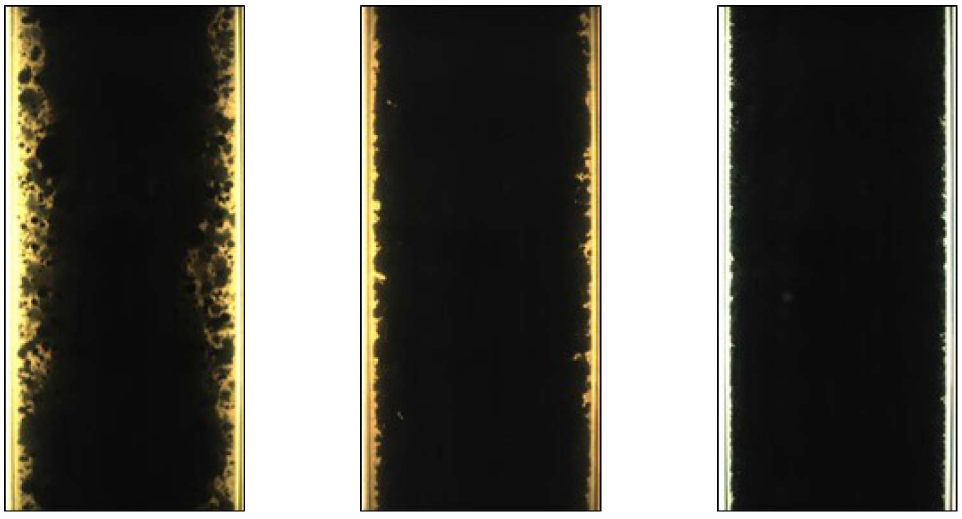

(a) @1561 cP and 29.16 °C (b) @1112 cP and 33.69 °C (c) @557 cP and 30.89 °C

Fig. 28. Two phase flow images for three different oil viscosities listed on Table 3-4 at oil and water superficial velocities of 0.8 and 0.6 m/s, respectively.

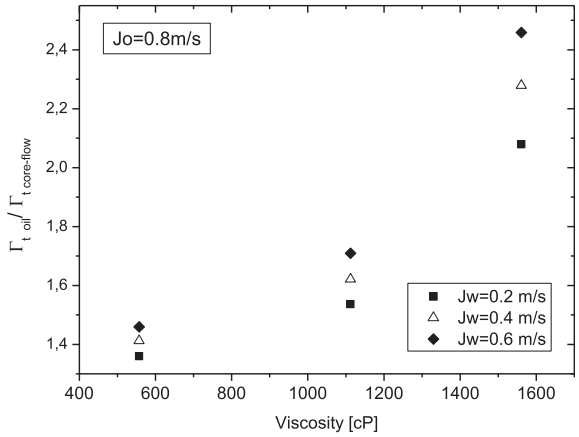

Fig. 29. Total reduction factor flow as a function of the oil viscosity.

Desenvolvimento" for the financial support. Acknowledgments are extended to ALFA Research Group and CEPETRO/UNICAMP.

References

[1] Agency, I. E. Resources to Reserves 2013 – Oil, Gas and Coal Technologies for the Energy Markets of the Future.
[2] J.D. Isaac, J.B. Speed. U.S. Patent No. 759,374. U.S. Patent and Trademark Office, Washington, DC, 1904.
[3] S. Abraham, A.F. Clark, U.S. Patent No. 2,533,878. U.S. Patent and Trademark Office, Washington, DC, 1950.
[4] T.W.F. Russell, M.E. Charles, The effect of the less viscous liquid in the laminar flow of two immiscible liquids, Can. J. Chem. Eng. 37 (1) (1959) 18–24.
[5] M.E. Charles, G.T. Govier, G.W. Hodgson, The horizontal pipeline flow of equal density oil-water mixtures, Can. J. Chem. Eng. 39 (1) (1961) 27–36.
[6] G. Ooms, The hydrodynamic stability of core-annular flow of two ideal liquids, Appl. Sci. Res. 26 (1) (1972) 147–158.
[7] R.V.A. Oliemans, The Lubricating-film Model for Core-annular Flow (Doctoral dissertation), Delft University of Technology, 1986.
[8] W.S. Ho, N.N. Li, Core-annular flow of liquid membrane emulsion, AIChE J. 40 (12) (1994) 1961–1968.
[9] A.C. Bannwart, Wavespeed and volumetric fraction in core annular flow, Int. J. Multiph. Flow 24 (6) (1998) 961–974.
[10] J.W.V. Prada, Estudo experimental do escoamento anular oleo-agua ("core flow") na elevação de oleos ultraviscosos, 1999.
[11] O.M.H. Rodriguez, Interfacial Shape and Pressure Gradient in Upward Vertical Core-Annular Flow. (Doctoral dissertation), State University of Campinas, 2002.
[12] J.L. Biazussi, Desenvolvimento de uma técnica de medida de vazão de óleo em escoamento bifásico do tipo core-flow, 2010.
[13] D.D. Joseph, et al., Core-annular flows, Annu. Rev. Fluid Mech. 29 (1) (1997) 65–90.
[14] R. Bai, Traveling waves in a high viscosity ratio and axisymmetric core annular flow. (PhD Thesis), University of Minnesota, 1995.
[15] W.L. Loh, V.K. Premanadhan, Experimental investigation of viscous oil-water flows in pipeline, J. Pet. Sci. Eng. 147 (2016) 87–97.
[16] H.Q. Zhang, C. Sarica, E. Pereyra, Review of high-viscosity oil multiphase pipe flow, Energy Fuels 26 (7) (2012) 3979–3985.
[17] J. Shi, L. Lao, H. Yeung, Water-lubricated transport of high-viscosity oil in horizontal pipes: the water holdup and pressure gradient, Int. J. Multiph. Flow 96 (2017) 70–85.
[18] W. Wagner, A. Pruß, The IAPWS formulation 1995 for the thermodynamic properties of ordinary water substance for general and scientific use, J. Phys. Chem. Ref. data 31 (2) (2002) 387–535.
[19] R.J. Moffat, Describing the uncertainties in experimental results, Exp. Thermal Fluid Sci. 1 (1) (1988) 3–17.
[20] O.M.H. Rodriguez, A.C. Bannwart, Experimental study on interfacial waves in vertical core flow, J. Pet. Sci. Eng. 54 (3–4) (2006) 140–148, ISSN 0920-4105, https://doi.org/10.1016/j.petrol.2006.07.007.
[21] A.C. Bannwart, et al., Flow patterns in heavy crude oil-water flow, J. Energy Resour. Technol. 126 (3) (2004) 184–189.